J Neurophysiol 90: 333–341, 2003.
First published February 26, 2003; 10.1152/jn.00715.2002.

Propagating Wave and Irregular Dynamics: Spatiotemporal Patterns of Cholinergic Theta Oscillations in Neocortex In Vitro

Weili Bao and Jian-Young Wu
Department of Physiology and Biophysics, Georgetown University, Washington DC, 20057-1421

Submitted 31 December 2002; accepted in final form 18 February 2003

Bao, Weili and Jian-Young Wu. Propagating wave and irregular dynamics: spatiotemporal patterns of cholinergic theta oscillations in neocortex in vitro. *J Neurophysiol* 90: 333–341, 2003. First published February 26, 2003; 10.1152/jn.00715.2002. Neocortical "theta" oscillation (5–12 Hz) has been observed in animals and human subjects but little is known about how the oscillation is organized in the cortical intrinsic networks. Here we use voltage-sensitive dye and optical imaging to study a carbachol/bicuculline induced theta (~8 Hz) oscillation in rat neocortical slices. The imaging has large signal-to-noise ratio, allowing us to map the phase distribution over the neocortical tissue during the oscillation. The oscillation was organized as spontaneous epochs and each epoch was composed of a "first spike," a "regular" period (with relatively stable frequency and amplitude), and an "irregular" period (with variable frequency and amplitude) of oscillations. During each cycle of the regular oscillation, one wave of activation propagated horizontally (parallel to the cortical lamina) across the cortical section at a velocity of ~50 mm/s. Vertically the activity was synchronized through all cortical layers. This pattern of one propagating wave associated with one oscillation cycle was seen during all the regular cycles. The oscillation frequency varied noticeably at two neighboring horizontal locations (330 μm apart), suggesting that the oscillation is locally organized and each local oscillator is about $\leq$300 μm wide horizontally. During irregular oscillations, the spatiotemporal patterns were complex and sometimes the vertical synchronization decomposed, suggesting a de-coupling among local oscillators. Our data suggested that neocortical theta oscillation is sustained by multiple local oscillators. The coupling regime among the oscillators may determine the spatiotemporal pattern and switching between propagating waves and irregular patterns.

INTRODUCTION

Oscillation in theta band (5–12 Hz) is a well-characterized activity in the mammalian brain. Hippocampal theta occurs exclusively during exploratory behaviors (Vanderwolf 1969) and rapid-eye movement sleep (Jovet 1969; Vanderwolf 1969), suggesting that this activity may be related to spatial learning and memory deposition. Neocortical theta activity has been observed in animal and human subjects (Raghavachari et al. 2001; Sarnthein et al. 1998) and may play a role in spatial learning and working memory (Lisman and Idiart 1995; Raghavachari et al. 2001). In vitro experiments indicate that at different phases of the oscillation, the same input to the local circuit may lead to different synaptic modifications (long-term potentiation or depression) (Huerta and Lisman 1995). Thus the phase distribution of the oscillation in the horizontal directions (parallel to cortical lamina) must play a role in determining when, where, and what synaptic modifications would occur in the cortical circuit.

The horizontal phase distribution over hippocampus was changing with behavior (O'Keef and Recce 1993; Skaggs et al. 1996), suggesting that cortical oscillators in CA3 and dentate gyrus may also contribute to the horizontal phase organization (Buzsaki 2002) in addition to the subcortical pacemaker neurons in the medial septum-diagonal band of Broca (Buzsaki et al. 1983; Lee et al. 1994; Leung 1984; Stewart and Fox 1990).

In neocortex, theta waves have been recorded during behavioral and mental tasks (Kahana et al. 1999; Raghavachari et al. 2001); however, almost nothing is known about the pace making and spatiotemporal organization of these waves.

An in vitro cholinergic oscillation (~7 Hz) can be generated in neocortical slices by bath applying of carbachol and bicuculline (Lukatch and MacIver 1997). This in vitro oscillation may share a common mechanism with the theta activity because applying these two agents together in vivo is sufficient to induce theta oscillations when the hippocampus is deafferented from the medial septum areas (Colom et al. 1991). These two agents may induce the oscillation by mimicking cholinergic depolarization (Benardo and Prince 1982; Cole and Nicoll 1984) and GABAergic disinhibition (Bilkey and Goddard 1985) of the assumed pacemakers. Under in vitro conditions, neocortical neurons do not receive any innervation from subcortical pacemaker(s). Thus the pacemaking and phase distribution must be organized by intrinsic neocortical oscillators.

In this report, we use voltage-sensitive dye (VSD) imaging to examine this in vitro neocortical oscillation. Pharmacologically generating the activity in brain slice allows us to exclude contributions from external (subcortical) pacemaker (s), allowing an analysis of how intracortical interactions organize the phase distribution.

In brain slices, the sensitivity of VSD imaging was high (Jin et al. 2002), allowing a simultaneously measurement from 50 to 100 locations over an area of ~4 mm in diameter. The advantage of optical recordings over an electrode array is that VSD imaging measures the transmembrane potentials of the neuronal population and thus the phase gradient caused by current source/sink pairs in the tissue is ignored, and only the phase in the membrane potential oscillation is measured. Our results show that the oscillation is organized as propagating waves. Local (~330 μm) phase variations suggest that the

Address for reprint requests: J.-Y. Wu, Georgetown University, Rm 247, Basic Science Building, 3900 Reservoir Rd. NW, Washington, DC 20057 (E-mail: wuj@georgetown.edu).

The costs of publication of this article were defrayed in part by the payment of page charges. The article must therefore be hereby marked "*advertisement*" in accordance with 18 U.S.C. Section 1734 solely to indicate this fact.

propagation wave may be composed of coupled local oscillators.

METHODS

Cortical slice preparation

Sprague-Dawley rats ($n = 20$) of both sexes from P28 to P35 were used. The animals were deeply anesthetized with halothane and quickly decapitated. The whole brain was chilled in cold (0–4°C) artificial cerebrospinal fluid [ACSF, containing (in mM) 132 NaCl, 3 KCl, 2 $CaCl_2$, 2 $MgSO_4$, 1.25 NaH_2PO_4, 26 $NaHCO_3$, and 10 dextrose and saturated with 95% O_2-5% CO_2] and coronal slices (450 μm thick) including occipital areas (Bregma −3 to −5 mm) were cut and transferred to a holding chamber for >60 min (at 22°C) before the next procedure.

VSD imaging

The imaging apparatus and methods are described in detail by Wu and Cohen (1993) and Jin et al. (2002). Briefly, the slices were stained with ACSF containing 0.005–0.02 mg/ml of an oxonol dye, NK3630 [first synthesized by R. Hildesheim and A. Grinvald as RH482; available from Nippon Kankoh-Shikiso Kenkyusho, Japan) (see Momose-Sato et al. (1999) for molecular structure], for 30–60 min (22°C). During staining, the dye solution was gently bubbled with 95% O_2-5% CO_2. The stained slices were then perfused in dye-free ACSF in a submerge chamber at 28–32°C during imaging experiments. A 124-element photodiode array system was used for the imaging. The preparation was *trans*-illuminated by 705 ± 20 nm light for the imaging. The illumination was only applied during recording trials (8–32 s each trial, >20 trials for each slice), and the exposure (light intensity and illumination time) did not cause detectable bleaching or phototoxicity (Jin et al. 2002). An objective of ×5 (0.12 NA, Zeiss) was used to form the image on the diode array. Each photodetector received light from an area of 330 × 330 μm^2 of the cortical tissue. With *trans*-illumination, neurons through the entire thickness of the slice (450 μm) contributed equally to the signal. The resting light intensity was $\sim 10^9$ photons/ms per detector and the VSD signal of the oscillation was $\sim 10^{-4}$ (peak-to-peak) of the resting light intensity. The signal was AC coupled at 0.1 Hz, amplified 200 times, low-pass filtered at 333 Hz, and then digitized at 1,000 frames/s with a 12-bit accuracy.

Local field potential recordings

Tungsten microelectrodes (epoxylite-coated, FHC, Bowdoinham, ME) with tip resistance of ~75 kΩ were used for sampling local field potentials. The electrode was carefully placed into the tissue so that the tissue surrounding the electrode produced normal VSD signals. The field potential signals were amplified ×1,000 and band-pass filtered at 0.1–400 Hz (by a Brownlee Precision 440 amplifier) and digitized at 1,000 Hz simultaneously with the VSD signals.

Data analysis and display

The optical data were analyzed using the program NeuroPlex (RedShirtImaging, LLC, Fairfield, CT). Data were displayed in the form of traces for numerical analysis and pseudocolor images for visualizing the spatiotemporal patterns. To generate pseudocolor maps, we normalized the signals from each individual detector to their own maximum amplitude (peak = 1 and baseline/negative peak = 0). Then a scale of 16 colors was linearly assigned to the values between 0 and 1 (Variable scaling in NeuroPlex). The pseudocolor maps were displayed as "contour" maps using the CONTOUR function provided by IDL (Interactive Data Language, Research Systems, Boulder, CO) and used by NeuroPlex.

RESULTS

Electrical and optical signals

When neocortical slices were perfused with 100 μM carbachol and 10 μM bicuculline at 28–32°C, oscillations at theta frequencies (5–14 Hz) occurred in the occipital area of the slice (Fig. 1) in agreement with the results obtained by Lukatch and MacIver (1997). These oscillations can be distinguished from epileptiform spikes in the same tissue: epileptiform spikes had high-amplitude (~1 mV) and low-repetition frequency (0.5–1.5 Hz), whereas theta oscillations had a low-amplitude (~0.5 mV) and high frequency (5–14 Hz) (Kowalczyk et al. 2001). Staining with the dye did not change the frequency, duration, or the amplitude of the theta oscillations recorded by the local field potential electrode (data not shown). During VSD imaging, only a moderate illumination intensity was used so that bleaching and photodynamic damage (resulting from high illumination intensity, Jin et al. 2002) were not detectable.

In cortical layer II–III, oscillations both in local field poten-

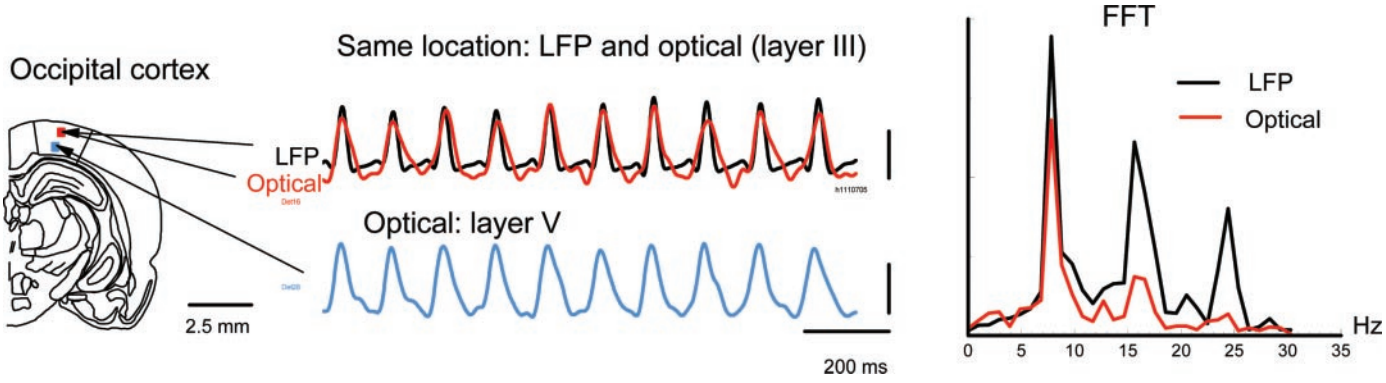

FIG. 1. *Left*: schematic diagram of the preparation and recording arrangement. Slices containing occipital cortex were sectioned from bregma −3 to −5 mm. A tungsten microelectrode was used to record local field potential (LFP) from cortical layer II–III. Voltage-sensitive dye (VSD) signals from the tissue surrounding the electrode (a volume of 330 × 330 × 450 μm^3, red square) were simultaneously recorded. *Middle*: in layer II–III, simultaneous electrical (black) and optical (red) recordings had a similar waveform during the oscillations. In layer V, the optical signal (blue) has the same polarity. Calibration bar: −50 μV for LFP and 10^{-4} for optical recordings. *Right*: power spectra of electrical (black) and optical (red) signals showed the same main peak at ~7.8 Hz during a sample piece (~20 cycles) of oscillations.

tial and optical signal were highly correlated in the same voxel ($330 \times 330 \times 450$ μm^3, Fig. 1, *middle, top 2 traces*). However, in local field recordings there were harmonic frequency components (Fig. 1, *right*). Local field potential signal has a continuous phase shift from Layers II–III to VI and opposite phases occurred in between superficial and deep layers (data not shown) (but see Fig. 7 of Lukatch and MacIver 1997). This phase reversal was not seen in the VSD recordings during most oscillation cycles (14 slices from 10 animals, 1 recording from layer V was shown in Fig. 1, *middle, bottom trace*, other examples are in Figs. 3*B*, and 5, *C3*, *C5*, and *D3*; an exception shown in Fig. 6*B*). This difference between electrodes and optical recordings demonstrated that VSD and field potential recordings measured different aspects of the neuronal activity. VSD signal is a population sum of transmembrane potential; Local field potential represents the local current density; the phase shift and polarity reversal indicate a current sink/source pair located in the cortical column (Lukatch and MacIver 1997). This phase shift is not present in the membrane potential oscillations. The phase map of VSD imaging correlates with the phase distribution in the membrane potential over the neuronal population without the interference of current source/sink pairs resulting from the geometrical arrangement of the neurons.

Oscillation epoch

This oscillation was organized in epochs. The epochs started spontaneously or could be triggered by an electrical stimulation (e.g., 0.5 V $\times$ 0.1 ms). In local field recordings, each epoch was composed of a large first spike (Fig. 2*B*), a period of "regular" cycles (relatively stable frequency and amplitude) followed by a period of "irregular" cycles (with variable frequency and amplitude, Fig. 2*B*). These three components were seen in all epochs, from five slices of five animals, with ~300 spontaneous epochs recorded from each slice by a local field potential electrode. When a large area of tissue was imaged optically, the three components could be more clearly characterized by their spatiotemporal patterns. When recorded with a single electrode from one point, there was no apparent activity before the first spike. With imaging we found that occasionally (2 of 47 epochs recorded optically, from 14 slices of 10 animals) the first spike was preceded by a local oscillation (Figs. 2*C*, 1, and 5*C*, 1). The first spike occurred as an excitation wave propagating across the tissue. After the first spike, the periodic activation spread to the whole field of view (Fig. 2*C*, image 1) and the frequency and amplitude became relatively stable (Fig. 2*C*, images 2 and 3). Each oscillation cycle was associated with one activation wave (comparing the traces and the image of Figs. 2*C*, image 2, and 3*A*). This one-cycle one-wave pattern was seen during the entire course of the oscillation. The oscillation frequency decreased from cycle to cycle (Figs. 2*C*, image 3, and Fig. 4*D*), and later the reoccurrence of the waves gradually became infrequent and "irregular", as the initiation site and propagating velocity varied in different cycles (Fig. 2*C*, images 5–7). The first cycle in Fig. 2*C*, image 5, started simultaneously on several detectors and propagated in the two opposite directions with different velocity. The second cycle in Fig. 2*C*, image 5, started from the bottom section and propagated up (a reversed direction as that in Fig. 2*C*, images 2–4). Complex patterns, such as collision and reflection of the waves also occurred: The first cycle in Fig. 2*C*, image 6, was initiated at the center of the tissue and propagates in both directions. Apparently the activity reflected at the edge of the field of view, and the reflected waves propagated back and collided in the center, forming an "O" pattern. Irregular periods were observed following regular cycles in all 47 epochs examined optically (14 slices from 10 animals). Other examples of irregular oscillations were documented in Figs. 5 and 6 and discussed in the related sections.

Propagating waves

During the regular oscillation period, VSD imaging revealed a localized activation associated with each oscillation cycle (e.g., Fig. 3*A*, pseudocolor images). The activated area had a columnar shape, perpendicular to the cortical laminae. The width of the active area (the area with signal >50% of the peak) was 400 ± 220 μm ($n = 15$). This activated area propagated continuously in the horizontal direction across the entire occipital cortex. "Propagating waves" were defined as one such activation wave correlated with one oscillation cycle (1-cycle 1-wave). The mean propagation velocity was 55 ± 21 mm/s (54 measurements from 54 waves in 3 slices). The horizontal propagation direction was the same (from medial to lateral, Figs. 2 and 5) during regular cycles.

During propagating waves, the activation of the neuronal population was more synchronized in the vertical (columnar) direction. Figure 3*B* shows the time difference for the VSD signal to reach its maximum at two neighboring detectors (named "peak-time difference" in this report). In the horizontal direction, the peak-time difference is centered around 6 ms, resulting from the propagation delay. In the vertical direction, the peak-time difference is centered around 0 ms. The shape of the distribution histogram in the vertical direction (red envelope in Fig. 3*B*) was also taller and thinner than that of the horizontal direction, indicating a better synchronization along the columnar direction than in the horizontal direction (also see Fig. 5*C*, 2 and 3). Because of this vertical synchronization, the propagating wave had a columnar shape in the activity maps (Fig. 3*A*, *bottom*).

Local frequency

Local oscillation frequency was examined on a spatial scale of ~330 μm. In Fig. 3*B*, the peak time difference at two horizontal neighboring locations had variations as large as $\pm$20 ms, suggesting a wide range of frequency variations within a 330-μm distance. Figure 4*A* shows the peak time difference of two neighboring detectors (330 μm apart, horizontally arranged in layer II–III, Fig. 4*B*) in consecutive cycles of a regular period of oscillation. The overall propagation direction was the same for all the cycles. The peak-time difference changed from cycle to cycle, from positive to negative values. In 14 slices (47 epochs) imaged optically, we found 11 detector pairs with continuous changing of local frequency (Fig. 4*C*, blue and black), whereas others have apparent random fluctuations (Fig. 4*C*, red). The continuous cycle-to-cycle change suggests that the local frequency variations were not randomly distributed nor caused by noises. Because the overall oscilla-

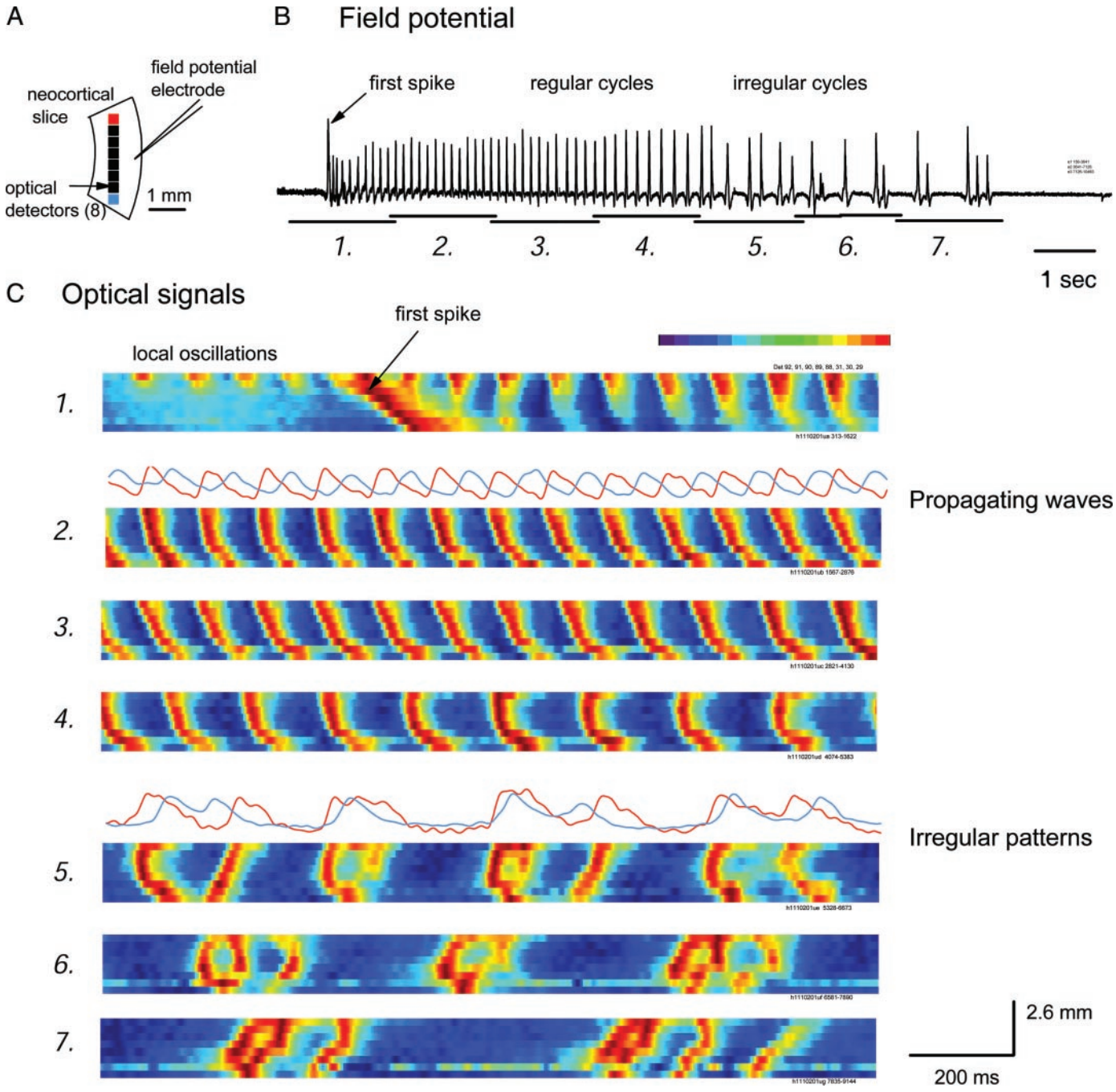

FIG. 2. Spatial-temporal patterns of a spontaneous oscillation epoch. *A*: recording arrangement. Signals from 8 optical detectors in deep cortical layers were used in *C*. A local field potential microelectrode was placed in layers II–III and recorded simultaneously with the optical imaging. *B*: an oscillation epoch recorded by the local field potential electrode. The epoch started spontaneously with a large first spike and followed by regular and irregular cycles. Optical signals during the period 1–7 (marked under the trace) of this epoch were shown in *C*. *C*: pseudocolor images composed from optical signals recorded by eight detectors arranged horizontally (shown in *A*). The optical signal from each detector was normalized to the maximum on that detector during that period and normalized values were assigned to colors according to a linear color scale (at the top right of *C*, 256 colors). The red and blue traces on top of the images 2 and 5 are optical signals from 2 optical detectors labeled red and blue in *A*. The *x* direction of the images is the time (~12 s) and the *y* direction of each image represents ~2.6 mm of space in cortical tissue. Note also that the first spike (*i*) had high amplitude but propagated slower in the tissue.

tion frequency declined with time (Fig. 4*D*), if in one location the frequency declined faster than its neighbors, continued peak-time variations would occur. This suggests that the frequency at two neighboring locations were at least partially controlled by two local oscillators. The local oscillators would have a size similar to or smaller than $330 \times 330\ \mu m^2$—the area of tissue imaged onto one optical detector.

Much larger local frequency variations were seen during irregular cycles where the oscillation at two neighboring locations can switch from phase advance to phase delay in one

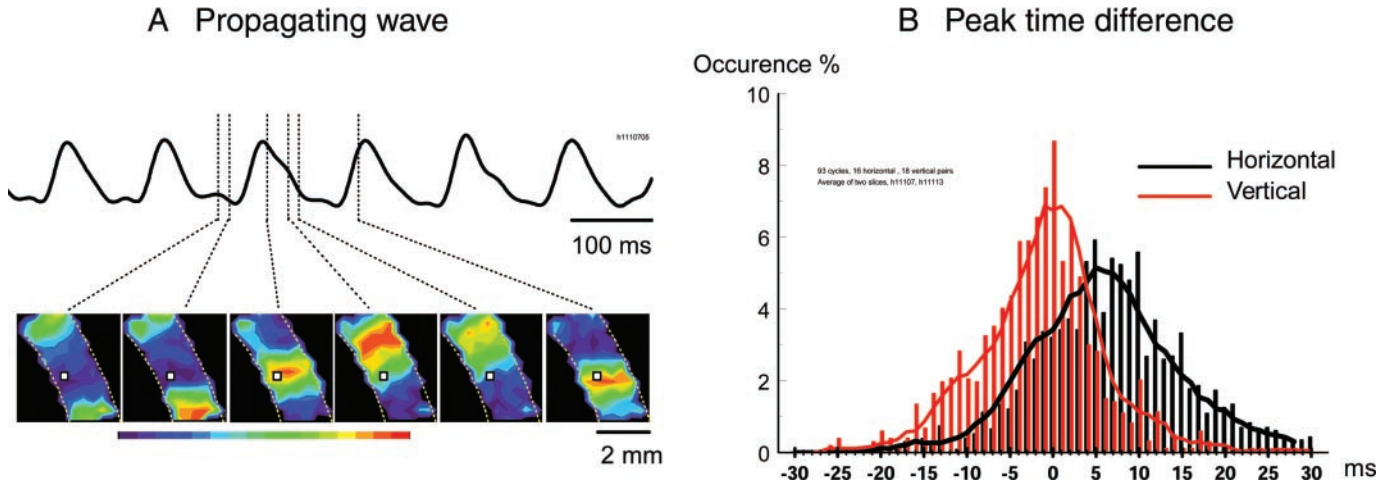

FIG. 3. *A*: propagating wave during the oscillation. Top: oscillation recorded from 1 optical detector in cortical layer V. The location of the detector is indicated by the small square in the images. *Bottom*: pseudocolor images synthesized from recordings of many optical detectors. The white broken lines mark the boundaries of the slice (Orientation: left, white matter; right, pia; top, medial, bottom, temporal). The images were 1-ms snap-shots chosen at times marked by the vertical broken lines. *B*: distribution of peak-time differences during 93 cycles of oscillation (2 slices from 2 animals). The bar chart is made from 3,162 measurements from 16 horizontal and 18 vertical pairs of measured points, all with a center-to-center distance of 330 μm. *y* axis: percentage of occurrences; *x* axis: delay time in ms. The envelope lines were generated by low-pass filtering of the bar chart data.

cycle. The irregular patterns were analyzed below to demonstrate that the horizontal coupling regime could break and local oscillators could activate independently.

Irregular oscillations

Examples of irregular oscillations from four different slices were shown in Fig. 5. In all the examples, propagating wave occurred before the irregular patterns, indicating that a coupling regime for regular propagating waves existed in all preparations, and this regime could degrade during the course of the epoch and dynamically change into other coupling patterns. The following irregular patterns were seen in the 14 slices we examined: *1*) dynamic reversal of propagating direction. The waves changed from the "\" to "/" shaped patterns in

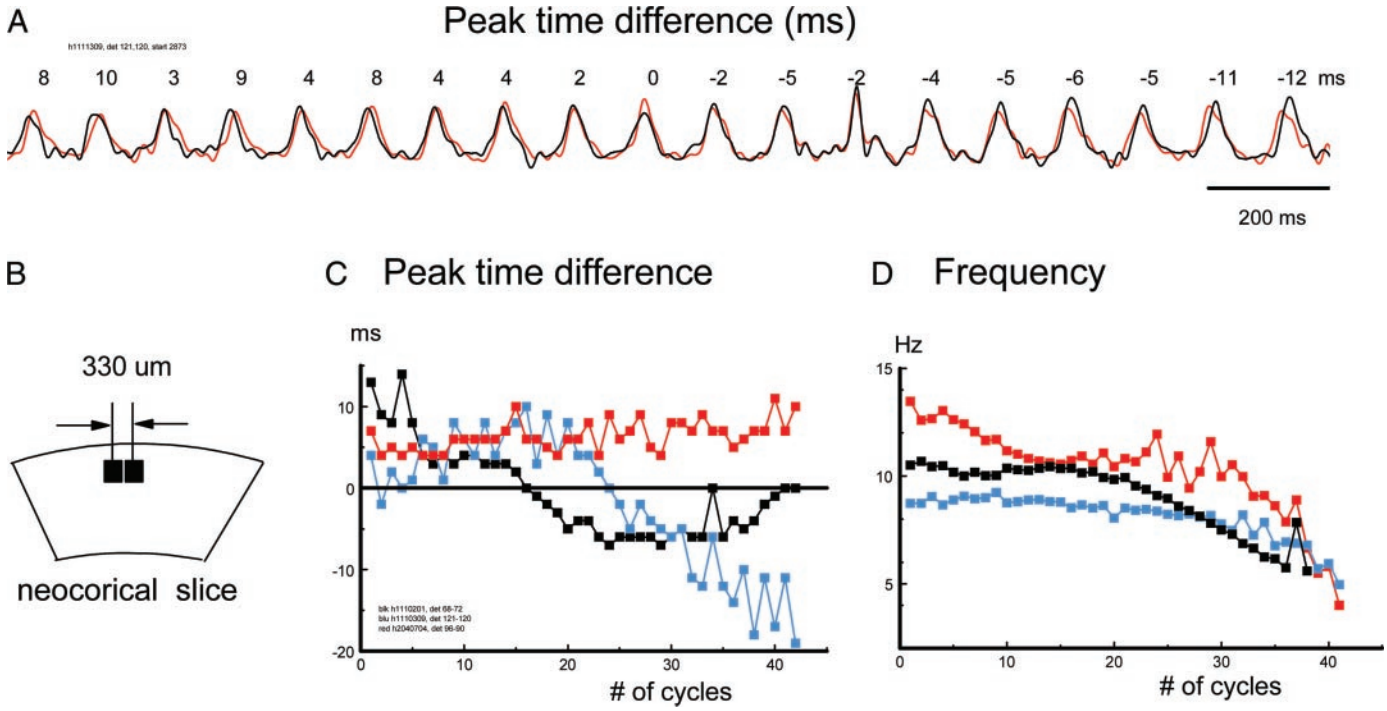

FIG. 4. Evidence of locally controlled frequency. *A*: oscillation cycles recorded from 2 neighboring optical detectors (red and black traces) with a horizontal separation of 330 μm (schematic diagram in *B*). The numbers on top of each cycle are the peak-time difference of that cycle. The peak-time difference decreased with time, from +8 to −12 ms, indicating that the frequency at 1 location (black) declined faster than that of the other location (red). *C*: variations of peak-time difference of three pairs of optical detectors (schematic in *B*) during regular oscillation cycles (from three animals). *D*: cycle-to-cycle variation of the frequency during the same periods as that shown in *C*.

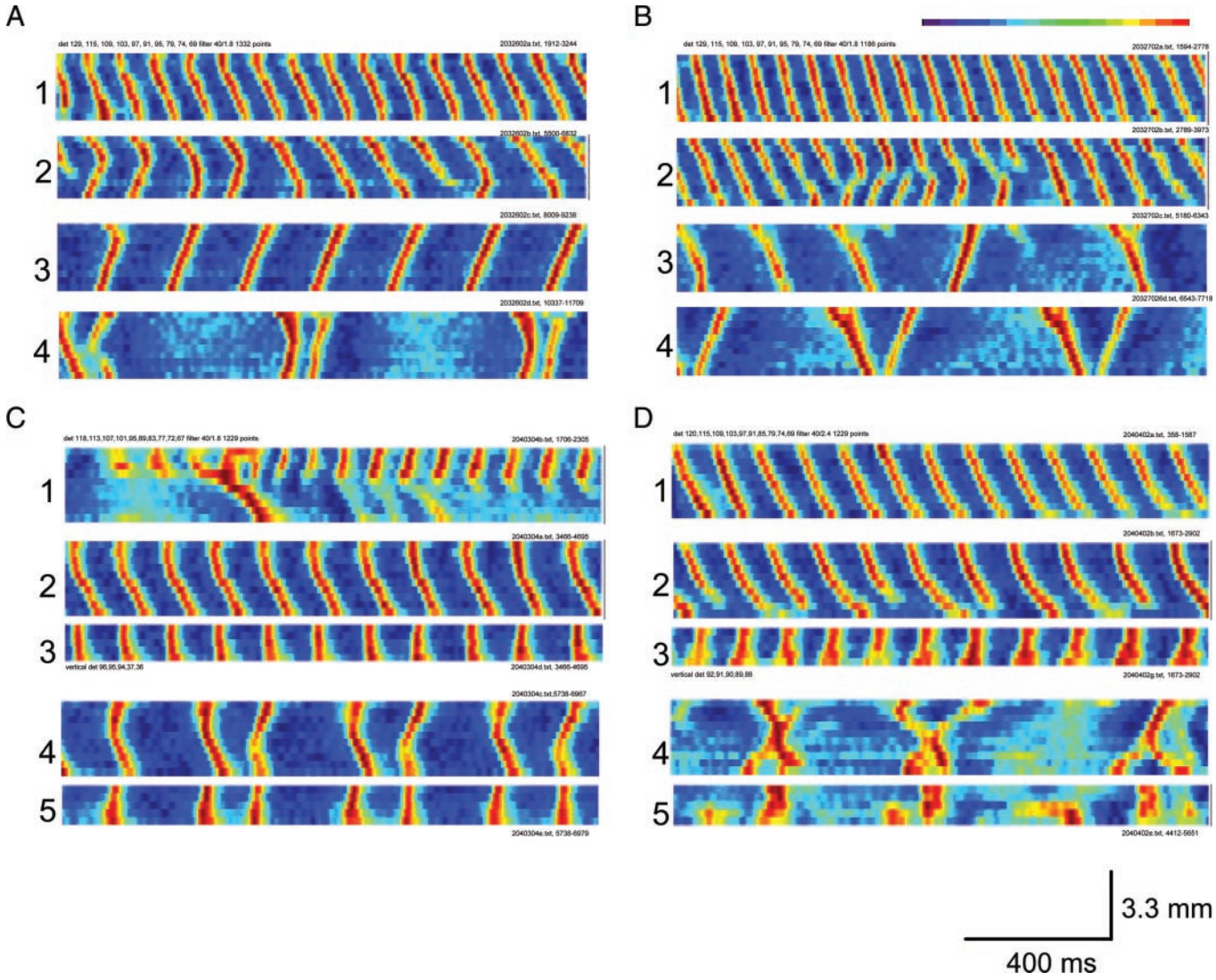

FIG. 5. Examples of irregular oscillations. *A–D*: data from 4 different animals. In each panel, all images were from the same epoch; however only part of regular and part of irregular cycles were shown. Images 3 and 5 in both *C* and *D* were from 5 vertically arranged detectors (total: 1.65 mm wide) between layers II (*top*) to VI (*bottom*), showing the vertical coupling during the same periods of images 2 and 4 in *C* and *D*, respectively. The rest of the images were from 10 detectors horizontally arranged (total: 3.3 mm wide) in cortical layers II–III. Each image showed a period of 12 s. Pseudo-color scale was linear, same as that for Fig. 2. See text for the descriptions of the patterns.

different cycles (Fig. 5*A*, images 1 and 3). When propagation direction changed, the phase relationship reversed in all neighboring locations; *2*) wave collision. Two waves propagated in opposite directions and collided in the middle, forming a "$>$" pattern (1st 4 cycles in image 2 of Fig. 5*A*); *3*) wave initiated in the center and propagated in two directions, forming a "$<$" pattern (1st cycle in image 4 of Fig. 5*C*); *4*) possible reflection of the wave occurred outside the field of view, forming a "V" shaped pattern (image 4 of Fig. 5*B*); and *5*) interruption of a propagating wave. In some cycles, the wave did not propagated through the entire tissue (image 2 of Fig. 5, *A* and *B*).

More complex patterns may be explained by the combination of the preceding patterns, such as the X-shaped pattern (image 4 of Fig. 5*D*), which can be explained as a combination of a collision and then the collision point initiating a new wave. The "O" shaped pattern (image 6 of Fig. 2*C*) can be explained as a combination of center initiation, reflections at both edges and then a collision at the center.

Vertical de-synchronization

As described before (Fig. 3, *A* and *B*), during propagating waves, the synchronization along cortical columns was better than that of horizontal (along the cortical laminae). Vertical synchronization also persevered during most irregular cycles when regular waves were disrupted (Fig. 5, *C*, 3 and 5, and *D*, 3). However, in the 14 slices we examined optically, we found two irregular periods where superficial and deep layers did not activate together. In one example during some irregular cycles, the activations in deep layers did not reach superficial layers (Fig. 5*D*, 5). In another slice (Fig. 6), the amplitude in layer II-III significantly reduced in some irregular cycles (Fig. 6*A*). Before these irregular cycles there was a period (Fig. 6*A*, $\times$) in which superficial and deep layers showed an alternating acti-

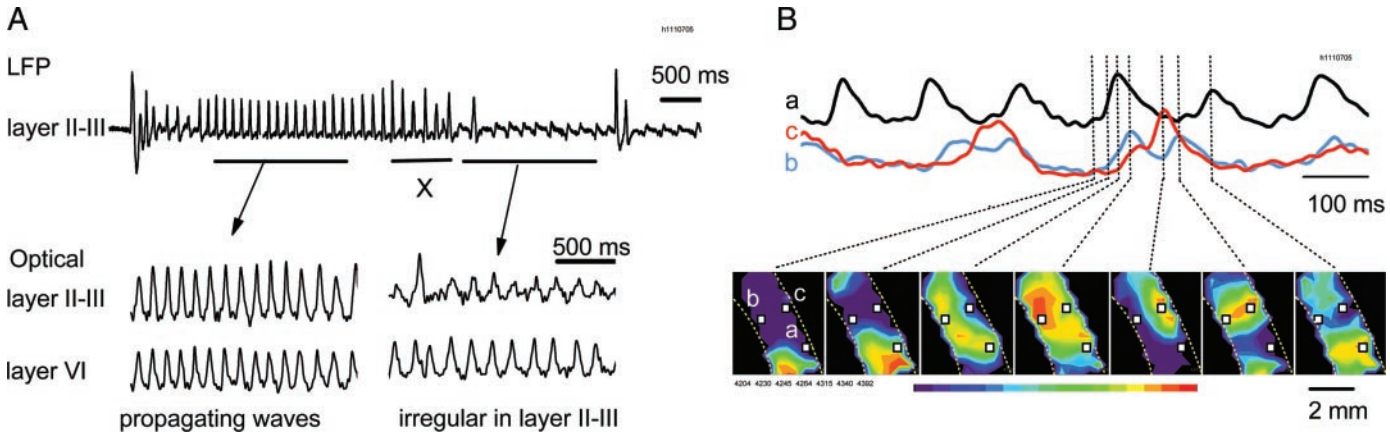

FIG. 6. Vertical de-synchronization. *A, top*: LFP recording of 1 epoch of oscillation. VSD imaging revealed periods of propagating waves (P) and irregular oscillations (I). R, activation with reversed propagation direction (data not shown). The period *x* is shown in detail in 4*B*. *Bottom*: VSD signals in layer II–III and V during different periods of the epoch. *B*: during irregular oscillations, the vertical synchrony decreased. VSD signals from different layers and locations showed different peak time and patterns.

vation. These examples suggest that superficial and deep layers of the same column may activate independently during the oscillation. However, vertical de-synchronization was much less frequently observed, suggesting that the coupling in the vertical direction is stronger that of the horizontal direction.

DISCUSSION

One-cycle one-wave

In this report we found that the in vitro cholinergic oscillation was organized as propagating waves. The oscillation has a one-cycle one-wave characteristic (Fig. 3); that is, each oscillation cycle is associated with one propagating wave. This characteristic was seen in the *N*-methyl-D-aspartate (NMDA) 7- to 10-Hz oscillation (Wu et al. 1999). The NMDA waves can be blocked by 2-amino-5-phosphonopentanoic acid (AP5) (Wu et al. 1999), but the cholinergic waves in this report were not blocked by AP5 (data not shown, see also Lukatch and MacIver 1997), suggesting that these propagating waves can be generated by more than one polysynaptic mechanisms. The propagating waves during the two oscillations had a similar velocity of 20–60 mm/s, slower than axonal conductance, suggesting both are mediated by polysynaptic local circuitry.

Propagating waves during oscillations were also observed in intact brains from turtle visual cortex (10–20 Hz) (Prechtl et al. 1997; Senseman and Robbins 1999) and olfactory bulb (5–30 Hz) (Lam et al. 2000) in response to natural sensory stimulation. In turtle visual cortex, the propagation waves also had a one-cycle one-wave characteristic but their spatial pattern was much more complex (Prechtl et al. 1997). Oscillations of different frequencies happened at the same time and travel in different directions (Prechtl et al. 1997). In intact cortex there are two horizontal dimensions that allow variations in many directions. In brain slices there is only one horizontal dimension and therefore only two possible propagation directions. Reversal in the propagation was observed in this cholinergic oscillation (e.g., Figs. 2*C*, 5, and 5*A*, 3) and also in the NMDA oscillations (7–10 Hz) where the horizontal direction reversed dynamically in different cycles (Fig. 7 of Wu et al. 1999). This dynamic change of propagation direction further suggests that the activation of the cortical neuron population is dynamically organized during the oscillation.

Coupled local oscillators and propagating waves

Our data suggest that the frequency of the oscillation may be determined by locally organized oscillators. Coupled local oscillators were also proposed during the evoked oscillations in turtle visual cortex (Prechtl et al. 2000). Mathematical models showed that propagating waves might emerge in a network of coupled oscillators with proper frequency gradient or coupling intensity (Ermentrout and Kopell 1984, 1994; Kopell 1988). In our data, the coupling intensity seemed to be variable in each epoch: During regular cycles, the phase relationship is less variable, suggesting a stronger coupling; during the irregular cycles following the regular period, the phase relationship was more variable suggesting a weaker coupling. In all slices, we found regular and irregular waves occurred in the same tissue, suggesting that the coupling intensity is controlled by dynamic factors of the local circuits because the anatomical connectivity did not change within seconds. However, anatomical connectivity may still play a role: in an examination of the waveforms in different cortical areas, Lukatch and MacIver (1997) reported irregular waveforms were often seen in somatosensory areas while regular oscillations were mostly seen in occipital and entorhinal cortices, suggesting different cortical areas may have different background coupling strengths.

In thalamic slices, the propagating patterns of spindle waves also have similar irregular patterns, such as collisions, multiple initiation points, and local waves (Kim et al. 1995). Other kinds of one-dimensional propagating waves formed by coupled oscillators have been suggested in developing chicken spinal cord (O'Donovan et al. 1998) and in the lamprey spinal cord during fictive swimming (Mellen et al. 1995; Rand et al. 1988). Coupled local oscillations may have complex behaviors (e.g., Davidenko et al. 1992). However, all the variety of propagating patterns observed (Figs. 2, 5, and 6) can be explained by the variations in the initiation site, collisions, and phase advance/delay between two neighboring locations.

Size of local oscillators

The optical signal originates from the change in transmembrane potential of neurons (Ross et al. 1977). Our signal is the averaged transmembrane potentials of many neurons. The estimated neuronal density in neocortical tissue is ~100,000 neuron/mm^3 (Douglas and Martin 1990). In the cortical tissue projected to one optical detector ($330 \times 330 \times 450$ μm^3), there were ~5,000 neurons. To detect the oscillation optically, a fraction of these neurons must change their membrane potential synchronously. Frequency fluctuations (Fig. 3) suggested that the size of the local oscillator is comparable to or less than the volume of the tissue ($330 \times 330 \times 400$ μm^3) projected onto one optical detector. Thus we estimate that the local oscillator during this cholinergic oscillation is organized with thousands of at least partially synchronized neurons.

During an evoked 20- to 80-Hz oscillation in cortical slices (Fig. 7 of Wu et al. 2001), the oscillation only appears on a field potential electrode but is not detectable optically from the same tissue, suggesting that the size of the local oscillator is substantially smaller than the volume of the tissue projected onto one optical detector. Another oscillation, a NMDA-mediated 7- to 10-Hz oscillation (Fig. 3 of Wu et al. 1999), can be detected optically, suggesting that it has larger local oscillators, similar to that of the cholinergic oscillation in this report.

Propagating velocity

The propagation velocity of excitation waves in neocortex has been measured during different population events (Bal et al. 1995; Chervin et al. 1988; Demir et al. 1999; Fleidervish et al. 1998; Golomb and Amitai 1997; Tanifuji et al. 1994; Tsau et al. 1998; Wu et al. 1999, 2001). GABAergic inhibition was proposed to be an important factor for controlling the propagating velocity of an excitation wave (Golomb and Ermentrout 2000). When the GABAergic network is intact, the propagation velocity of the evoked gamma oscillation is ~10 mm/s (Wu et al. 2001). After blocking $GABA_A$ receptors with bicuculline, the propagation velocity increased to ~130 mm/s (Wu et al. 2001). Here we show that in the presence of carbachol and bicuculline, the propagation velocity was much slower than that of adding bicuculline alone. We speculate that carbachol might modify the network to form localized oscillators and that the slow propagation wave may be due to network localization and the phase lags between neighboring oscillators.

Conclusions

Our results suggest that propagating waves during neocortical oscillations are organized by coupled local oscillators. Each oscillator is a population unit, composed of thousands of neurons. Variation in the coupling strength may contribute to the spatiotemporal dynamics of the waves. A number of questions remain. What defines a population oscillator? What determines the coupling strength? Finally, do similar oscillations also occur in vivo? The wavelengths of the propagating waves were small (~4 mm, Figs. 3). It might be difficult for scalp electroencephalgraphy to reach such a high spatial resolution (Ferree and Clay 2000) and detect waves with such small wavelengths. Additional experiments will be needed to address these questions.

We thank Drs. L. B. Cohen, G. B. Ermentrout, and J. E. Lisman for helpful comments.

This work was supported by National Institute of Neurological Disorders and Stroke Grant NS-36477 and a Whitehall Foundation grant.

REFERENCES

Bal T, Von Krosigk M, and McCormick DA. Synaptic and membrane mechanisms underlying synchronized oscillations in the ferret lateral geniculate nucleus in vitro. *J Physiol* 483: 641–663, 1995.

Benardo LS and Prince DA. Cholinergic pharmacology of mammalian hippocampal pyramidal cells. *Neuroscience* 7: 1703–1712, 1982.

Bilkey DK and Goddard GV. Medial septal facilitation of hippocampal granule cell activity is mediated by inhibition of inhibitory interneurones. *Brain Res* 361: 99–106, 1985.

Bragin A, Jando G, Nadasdy Z, Hetke J, Wise K, and Buzsaki G. Gamma (40–100 Hz) oscillation in the hippocampus of the behaving rat. *J Neurosci* 15: 47–60, 1995.

Buzsaki G. Theta oscillations in the hippocampus. *Neuron* 33: 325–340, 2002.

Buzsaki G, Leung LW, and Vanderwolf CH. Cellular bases of hippocampal EEG in the behaving rat. *Brain Res* 287: 139–171, 1983.

Chervin RD, Pierce PA, and Connors BW. Periodicity and directionality in the propagation of epileptiform discharges across neocortex. *J Neurophysiol* 60: 1695–1713, 1988.

Cole AE and Nicoll RA. The pharmacology of cholinergic excitatory responses in hippocampal pyramidal cells. *Brain Res* 305: 283–290, 1984.

Colom LV, Nassif-Caudarella S, Dickson CT, Smythe JW, and Bland BH. In vivo intrahippocampal microinfusion of carbachol and bicuculline induces theta-like oscillations in the septally deafferented hippocampus. *Hippocampus* 1: 381–390, 1991.

Davidenko JM, Pertsov AM, Salomonsz R, Baxter WP, and Jalife J. Spatiotemporal irregularities of spiral wave activity in isolated ventricular muscle. *J Electrocardiol* 24: 113–122, 1992.

Demir R, Haberly LB, and Jackson MB. Sustained and accelerating activity at two discrete sites generate epileptiform discharges in slices of piriform cortex. *J Neurosci* 19: 1294–1306, 1999.

Douglas RJ and Martin KAC. Neocortex. In: *The Synaptic Organization of the Brain*, edited by Shepherd GM. New York: Oxford, 1990, p. 401–435.

Ermentrout GB and Kopell N. Frequency plateaus in a chain of weakly coupled oscillators. *SIAM J Appl Math* 15: 215–237, 1984.

Ermentrout GB and Kopell N. Inhibition-produced patterning in chains of coupled nonlinear oscillators. *SIAM J Appl Math* 54: 478–507, 1994.

Ferree T and Clay M. Lead field theory and the spatial sensitivity of scalp EEG. Technical Note, Electrical Geodesics, http://www.csi.uoregon.edu/members/ferree/tutorials/LeadFieldTheory.pdf, 2000.

Fleidervish IA, Binshtok AM, and Gutnick MJ. Functionally distinct NMDA receptors mediate horizontal connectivity within layer 4 of mouse barrel cortex. *Neuron* 21: 1055–1065, 1998.

Golomb D and Amitai Y. Propagating neuronal discharges in neocortical slices: computational and experimental study. *J Neurophysiol* 78: 1199–1211, 1997.

Golomb D and Ermentrou GB. Effects of delay on the type and velocity of travelling pulses in neuronal networks with spatially decaying connectivity. *Network* 11: 221–46, 2000.

Huerta PT and Lisman JE. Bidirectional synaptic plasticity induced by a single burst during cholinergic theta oscillation in CA1 in vitro. *Neuron* 15: 1053–1063, 1995.

Jin WJ, Zhang RJ, and Wu JY. Voltage-sensitive dye imaging of population neuronal activity in cortical tissue. *J Neurosci Methods* 115: 13–27, 2002.

Jovet M. Biogenic amines and the states of sleep. *Science* 163: 32–41, 1969.

Kahana MJ, Sekuler R, Caplan JB, Kirschen M, and Madsen JR. Human theta oscillations exhibit task dependence during virtual maze navigation. *Nature* 399: 781–784, 1999.

Kopell N. Toward a theory of modelling central pattern generators. In: *Neurocontrol of Pythmic Movements in Vertebrates*, edited by Coehn AH, Rossignal S, and Grillner S. New York: Wiley, 1988.

Kowalczyk T, Golebiewski H, Eckersdorf B, and Konopacki J. Window effect of temperature on carbachol-induced theta-like activity recorded in hippocampal formation in vitro. *Brain Res.* 901: 184–194, 2001.

Kim U, Bal T, McCormick DA. Spindle waves are propagating synchronized oscillations in the ferret LGNd in vitro. *J Neurophysiol* 74:3 1301–1323, 1995.

Lam YW, Cohen LB, Wachowiak M, and Zochowski MR. Odors elicit three different oscillations in the turtle olfactory bulb. *J Neurosci* 20: 749–762, 2000.

Lee MG, Chrobak JJ, Sik A, Wiley RG, and Buzsaki G. Hippocampal theta activity following selective lesion of the septal cholinergic system. *Neuroscience* 62: 1033–1047, 1994.

Leung LS. Theta rhythm during REM sleep and waking: correlations between power, phase and frequency. *Electroencephalogr Clin Neurophysiol* 58: 553–564, 1984.

Lisman JE and Idiart MA. Storage of 7 +/- 2 short-term memories in oscillatory subcycles. *Science* 267: 1512–1515, 1995.

Lukatch HS and MacIver MB. Physiology, pharmacology, and topography of cholinergic neocortical oscillations in vitro. *J Neurophysiol* 77: 2427–2445, 1997.

Mellen N, Kiemel T, and Cohen AH. Correlational analysis of fictive swimming in the lamprey reveals strong functional intersegmental coupling. *J Neurophysiol* 73: 1020–1030, 1995.

Momose-Sato Y, Sato K, Arai Y, Yazawa I, Mochida H, and Kamino K. Evaluation of voltage-sensitive dyes for long-term recording of neural activity in the hippocampus. *J Membr Biol* 172: 145–157, 1999.

O'Donovan MJ, Wenner P, Chub N, Tabak J, and Rinzel J. Mechanisms of spontaneous activity in the developing spinal cord and their relevance to locomotion. *Ann NY Acad Sci* 860: 130–141, 1998.

O'Keefe J and Recce ML. Phase relationship between hippocampal place units and the EEG theta rhythm. *Hippocampus.* 3: 317–330, 1993.

Prechtl JC, Bullock TH, and Kleinfeld D. Direct evidence for local oscillatory current sources and intracortical phase gradients in turtle visual cortex. *Proc Natl Acad Sci USA* 97: 877–882, 2000.

Prechtl JC, Cohen LB, Pesaran B, Mitra PP, and Kleinfeld D. Visual stimuli induce waves of electrical activity in turtle cortex. *Proc Natl Acad Sci USA* 94: 7621–7626, 1997.

Rand RH, Cohen AH, Holmes PJ. Systems of coupled oscillators as models of central pattern generators. In: *Neurocontrol of Pythmic Movements in Vertebrates,* edited by Cohen AH, Rossignal S, and Grillner. New York: Wiley, 1988.

Raghavachari S, Kahana MJ, Rizzuto DS, Caplan JB, Kirschen MP, Bourgeois B, Madsen JR, and Lisman JE. Gating of human theta oscillations by a working memory task. *J Neurosci* 21: 3175–3183, 2001.

Ross WN, Salzberg BM, Cohen LB, Grinvald A, Davila HV, Waggoner AS, and Wang CH. Changes in absorption, fluorescence, dichroism, and Birefringence in stained giant axons: optical measurement of membrane potential. *J Membr Biol* 33: 141–183, 1977.

Sarnthein J, Petsche H, Rappelsberger P, Shaw GL, and von Stein A. Synchronization between prefrontal and posterior association cortex during human working memory. *Proc Natl Acad Sci USA* 95: 7092–7096, 1998.

Senseman DM and Robbins KA. Modal behavior of cortical neural networks during visual processing. *J Neurosci* 19: RC3, 1999.

Skaggs WE, McNaughton BL, Wilson MA, and Barnes CA. Theta phase precession in hippocampal neuronal populations and the compression of temporal sequences. *Hippocampus.* 6: 149–172, 1996.

Stewart M and Fox SE. Do septal neurons pace the hippocampal theta rhythm? *Trends Neurosci* 13: 163–168, 1990.

Tanifuji M, Sugiyama T, and Murase K. Horizontal propagation of excitation in rat visual cortical slices revealed by optical imaging. *Science* 266: 1057–1059, 1994.

Tsau Y, Guan L, and Wu JY. Initiation of spontaneous epileptiform activity in the neocortical slice. *J Neurophysiol* 80: 978–982, 1998.

Vanderwolf CH. Hippocampal electrical activity and voluntary movement in the rat. *Electroencephalogr Clin Neurophysiol* 26: 407–418, 1969.

Wu JY and Cohen LB. Fast multisite optical measurement of membrane potential. In: *Biological Techniques: Fluorescent and Luminescent Probes for Biological Activity,* edited by Mason WT. New York: Academic, 1993, p. 389–404.

Wu JY, Guan L, Bai L, and Yang Q. Spatiotemporal properties of an evoked population activity in rat sensory cortical slices. *J Neurophysiol* 86: 2461–2474, 2001.

Wu JY, Guan L, and Tsau Y. Propagating activation during oscillations and evoked responses in neocortical slices. *J Neurosci* 19: 5005–5015, 1999.